Enhanced microwave absorption property of aluminum composites using fly ash derived cenosphere

Rajeev Kuma[1*,2], D.P. Mondal[1,2], Shyam Birla[1,2], Amit Vishwakarma[1], Anisha Chaudhary[3], Saroj Kumari[3] and S. Das[1]

[1]*Division of Light Weight Metallic Materials, CSIR-Advanced Materials and Processes Research Institute, Near Habibgang Naka, Bhopal 462026, MP, India*
[2]*Academy of Scientific and Innovative Research (AcSIR), Taramani, Chennai 600113, Tamil Nadu, India*
[3]*Advanced Materials and Devices Division, CSIR-National Physical Laboratory, Dr. K.S. Krishnan Road, New Delhi 110012, India*

[*]Corresponding author

DOI: 10.5185/amlett.2018.1760
www.vbripress.com/aml

Abstract

In the present investigation, influence of micronsize cenosphere particles derived from fly ash on the properties of aluminum composites was investigated. Aluminum-cenosphere (AC) composite was fabricated by modified stir casting technique. The mechanical and electromagnetic interference (EMI) shielding properties of AC composites were investigated. The obtained composites with cenosphere (+100 µm) loading demonstrate the excellent compressive strength of 251.3 MPa. This enhancement is due to the smaller size of cenosphere size provides the finer surface of the cenosphere. The addition of cenosphere in aluminum matrix improved dielectric and microwave absorption properties of composites in X band frequency region (8.2-12.4 GHz). The AC composites possess good EMI shielding effectiveness of -32.7 to -44.3 dB with 30% loading of cenosphere with various sizes (+212, +150 and +100 µm). The incorporation of lower size cenosphere (+100µm) in aluminum matrix significantly increases the interfacial polarization which leads to a higher absorption EMI shielding effectiveness (SE) of -31.1 dB at 2.0 mm thickness. This technique is very simple, economical and highly reproducible, which may facilitate the commercialization of such composite and it can be used as microwave absorbing materials in defense and aerospace applications.

Keywords: Aluminum alloy, cenosphere, composites, compressive strength, microwave absorption, EMI shielding.

Introduction

With increasing the use of a large number of wireless gadgets in the contemporary technological world and related electromagnetic (EM) radiation is becoming a serious problem which can disturb electrical circuits, cell phones, televisions, satellite communications and may harm to a human being [**1**-**3**]. In civil and military aerospace vehicles, protection from EM radiations as well as control of thermal heating of electronic power systems is necessary to protect them from any form of damages. In specific, high shielding materials are needed to moderate EM interference (EMI) from electronic systems and to protect human from hazards of space radiation [**4, 5]**. The EMI attenuation offered by a shield depends upon three mechanisms; a reflection of the incident radiation from the shield's face, absorption of the un-reflected radiation as it passes through the shield and re-reflection i.e. multiple reflections of the waves at various interfaces within the shield material [**6**]. In case of reflection of the radiation by the shielding material, the shield material must have mobile charge carriers (electron or holes), which interact with the EM field in the radiation. As a result, the shield material tends to be electrically conducting. Traditional materials such as boron, tungsten, titanium, nickel, tantalum, silver, gold, copper, aluminum or some combination of these materials possessing high conductivity and dielectric constant are considered to be the best conventional EMI shielding materials with high shielding effectiveness [**1, 7**]. However, these metals have disadvantages like high density, easy corrosion and higher cost, which restrict their use as EMI shielding materials. Furthermore, these metals are the most common materials for reflection due to the free electrons in them. For aerospace transportation vehicles and space structures application, materials should have high absorption rather than reflection since reflected wave might disturb another electronic system [**8, 9**]. Additionally, absorption of shield material depends on the electric or magnetic dipoles, which interact with the electromagnetic field of the radiation. Among the different materials, aluminum composites have emerged as a promising candidate for EMI shielding owing to its outstanding properties such as low density, high electrical/thermal transport and

mechanical properties [**10, 11**]. It has been reported that aluminum composites have good EMI shielding performance (mainly reflection dominant) within the frequency range of 100-2000 MHz but the shielding mechanism of aluminum composites have not been studied in X- band (8.2-12.4 GHZ) frequency region [**12, 13**]. Additionally, contribution of absorption and reflection have not been studied. Furthermore, EMI shielding with high absorption performance depends upon many factors like structure, compositions and filling materials which are used in the fabrication process. So far, a wide range of magnetic nanoparticles such as Fe, Ni, Co ferrites and their multi-component ferrites like Fe_2O_3, Fe_3O_4, CrO_2 [**14-16**] and dielectric nanoparticles like MnO_2, ZnO, SiO_2 and fly ash cenosphere [**17-24**] have been reported for high absorption. Among all of them, fly ash cenosphere has been found to be more efficient absorbing material. Fly ash cenosphere are solid-waste by-products of power generating thermal plants and are pollutants [**25,26**]. Recently, cenospheres incorporated polymer or cement matrix composite for EMI shielding properties have been paid great attention. Metal coated cenospheres has been proposed by many researchers in order to act as a magnetic waves shield against the electromagnetic radiations and used as EMI shielding material for electronic and radar application [**13,27]**. Furthermore, cenospheres incorporated aluminum-alloy matrix to enhance the EMI shielding properties of the composite is also reported in literatures [**28**]. Therefore, we have selected the cenospheres as dielectric filler in aluminum alloy composite. Cenospheres being hollow and spherical will entrapped within the aluminum matrix and increases the interfacial area and porosity of the composite. Additionally it will not add up the much weight to the composite even at high loading. Hence, the light weight of the composite will be maintained and its cost will be reduced. Moreover, the dielectric constituents present in the cenospheres like SiO_2 and Al_2O_3 [**29**] will help in improving the dielectric loss properties of the aluminum composite. Furthermore, due to the ceramic spherical surface, there are more chances of reflection of electromagnetic waves through the surface which will reflect again and again from the surface of cenospheres, stuck inside the network structure of the composite.

In the present effort, cenosphere was used to improve the mechanical strength with high absorption of the aluminum composite by varying the size of cenosphere particles. The aluminum-cenosphere (AC) composites were developed using cenosphere of different size (+212, +150 and +100 μm) as a reinforcement. To ascertain the effect of cenosphere and its decreasing size on aluminum composites are characterized by scanning electron microscopy, X-ray diffraction, vector network analyzer for EMI shielding and compressive strength.

Experimental

Material preparation

AC composite was prepared using modified stir casting technique [30]. For the development of composites, the first LM13 aluminum alloy was melt at ~700°C in an electrical resistance furnace and 30 vol. % of pre-heated cenosphere with three different sizes (+100, +150 and +212μm) were mixed with the help of mechanical stirrer. The liquid mixture (i.e. aluminum-cenosphere composites) was cast in a cylindrical cast iron die of 20 mm diameter and 200 mm height. The mold is cooled with forced air to avoid floating of cenosphere in the die. It also helps in reducing the pushing phenomena of cenosphere by the solidification front and helps in getting more uniform distribution. The composites made with +212μm (average size 256 ± 25μm), +150μm (average size 165 ± 15μm) and +100 μm (average size 128 ± 14μm) size cenosphere were named as ACC212, ACC150 and ACC100 respectively. The schematic representation for fabrication aluminum-cenosphere composites is given in supporting information **(Fig. S1)**.

Characterization

Surface morphology of cenosphere and AC composites was studied by scanning electron microscope (SEM, JEOL: model: 5600) operating at 10 kV. X-ray diffraction (XRD) studies of the samples were performed in the scattering range of 10–80° at a scanning rate of 0.01°/min on D-8 Advanced Bruker diffractometer using CuKa radiation (λ=1.5418Å). Compressive strength or stress and strain behavior of composites were measured using Instron Universal Testing Machine (INSTRON UTM, Model 8801) at the strain rate of 0.01/s using cylindrical samples of 10 mm diameter and 15 mm length. EMI-Shielding effectiveness in the frequency range of 8.2–12.4 GHz (X-band) was measured at room temperature by waveguide using vector network analyzer (VNA E8263B Agilent Technologies). For EMI SE, AC composites samples were cut in a rectangular shape of dimension dimensions 26.8X13.5 X2.0 mm to fit within the cavity of the sample holder. A full two-port calibration was performed using a quarter-wavelength offset and termination and keeping the input power level at -5.0 dBm.

Results and discussion

Fig. 1 (a-f) shows the SEM image of cenosphere and AC composites with various size. **Fig. 1 (a)** represents the SEM image of cenosphere (size+100μm) it is clearly evident that the surface of cenosphere is smooth and the sizes of cenosphere particles are uniform in shape with mean size 128 μm. There are some white spots in the center of cenosphere from the image, which is considered to be caused by the accumulation of electric charge on the cenosphere during SEM imaging. The surface becomes relatively smoother when the cenosphere size is lower. It is also noted that the density of cenosphere is almost same irrespective of the cenosphere size. It is assumed that some of the cenospheres get fragmented during stirring and **Fig. 1 (b)** represent the SEM image of as received crushed cenosphere (+100μm). **Fig. 1 (c)** shows the microstructure of ACC212 and indicates that cenosphere particles are distributed uniformly within the Al-alloy.

Fig. 1 (d) shows high magnified image of ACC212 indicating the sharp interface between cenosphere shell and the aluminum matrix. The higher size of cenosphere with highly porous shell structure has the possibility of breaking during mechanical stirring and may decrease the compressive strength of the ACC212. The microstructures of ACC150 and ACC100 as shown in **Fig. 1 (e) and (f)** respectively also depicted the uniform distribution of cenosphere. It is assumed that lower size of cenosphere did not break during mixing and thus it is expected that the average cenosphere size in composites will be almost same as that was in as-received condition.

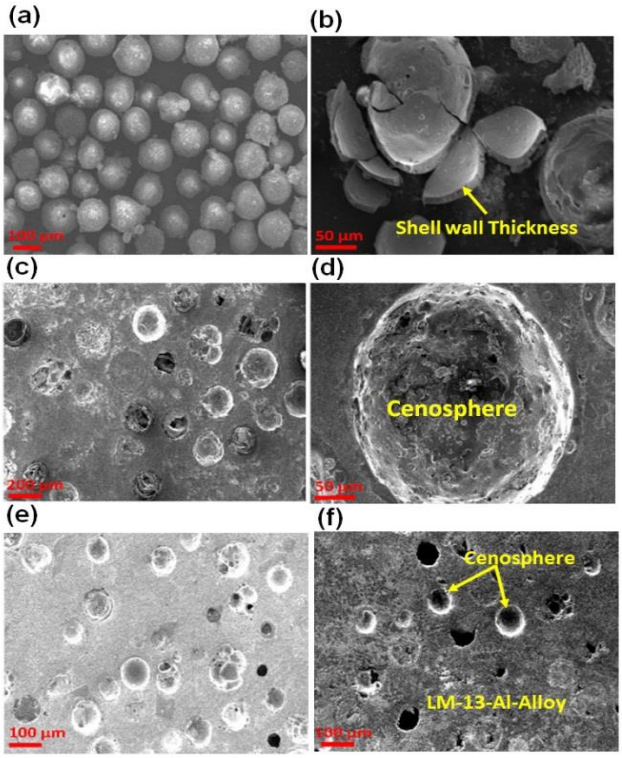

Fig. 1. SEM micrographs of (a) cenosphere, (b) fragmented cenosphere, (c) AC composites (ACC212), (d) cenosphere in aluminum matrix (ACC212), (e) ACC150 and (f) ACC100.

Uniform distribution is caused due to (i) spherical nature of particles and (ii) presence of silicates or silicon oxide in cenosphere which improves its wettability with aluminum matrix. The lower size of cenosphere (+100 µm) in ACC100 indicates strong bonding between cenosphere shell and the matrix alloy. Furthermore, lower size of cenosphere have the surface smoother and also showed that the eutectic silicon is concentrated around the boundary of cenospheres, this is due to dissolution of SiO_2 which is reduced to Si by aluminum, and also due to pushing of cenosphere by the solidification front, therefore, the compressive strength of ACC100 may be higher. However, in ACC212, the cenospheres are quite large and its diameter is significantly larger, the larger diameter of cenosphere particles may cause agglomeration or dendrite formation in an aluminium matrix, this is responsible for decreasing properties of the composites.

Fig. 2 (a) demonstrates typical X-ray diffraction pattern of cenosphere particles and **Fig. 2 (b)** shows the XRD of composites (ACC100). In **Fig. 2 (a)** various diffraction peaks for cenosphere are observed at a 2θ angle which represents that the cenosphere primarily contains alumino-silicate phases like mullite and sillimanite and other minor phases like ferrosilicates and quartz. Besides these phase constituents, the major phases are mullite and sillimanite. The incorporation of cenosphere influences the crystallographic structure of aluminum alloy, as a result peak position also changes as appeared in **Fig. 2 (b)**. XRD analysis indicates that there is the possibility of chemical reactions between the aluminum melt and cenosphere during solidification processing at a temperature above the melting temperature of aluminum [**30**].

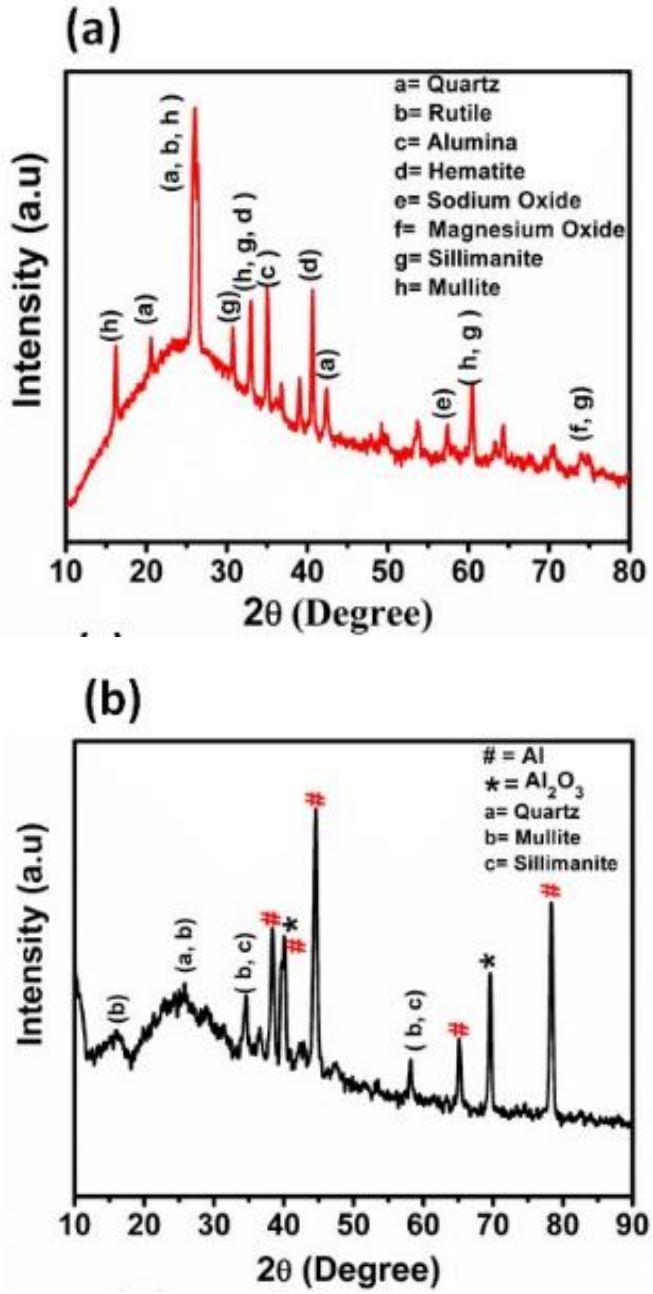

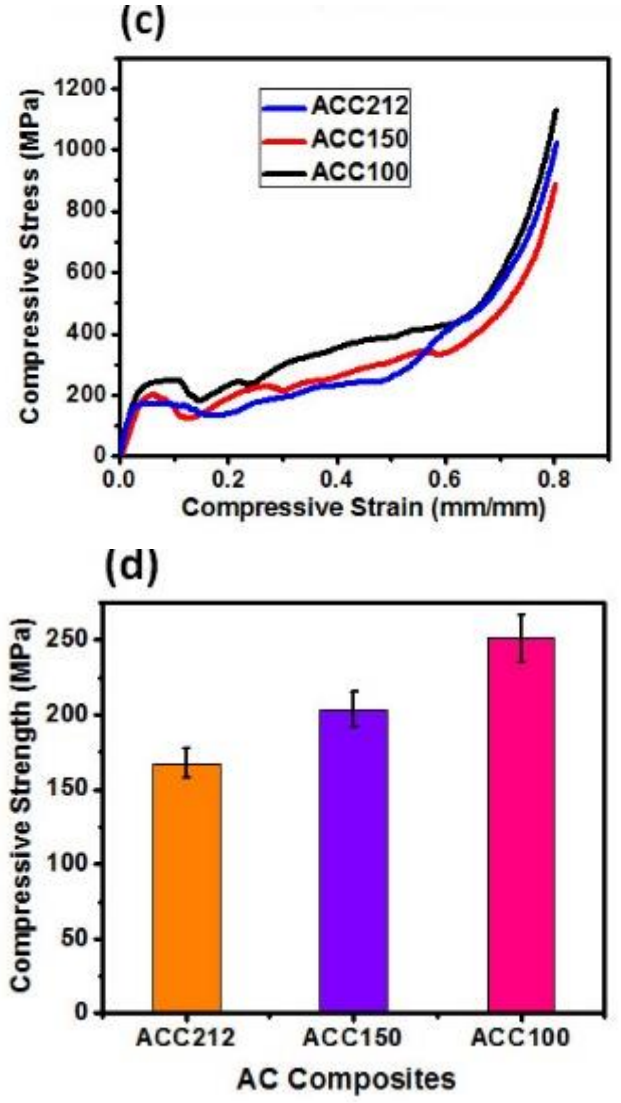

Fig. 2. XRD patterns of (a) cenosphere, (b) AC composites (ACC100), (c) compressive stress-strain curve and (d) compressive strength of AC composites.

The volume fraction of cenosphere in the AC composite was 30 % and the porosity within cenosphere are in the range of 70 to 72%, thus it is expected that the density of the composite would be around 27 to 29 % less than that of the alloy. The density of the composites is around 1.88 to 1.98 g/cm^3.

The measured value of density, relative density (RD) and porosity are reported in the **Table 1**.

Table 1. Density and porosity of AC composites.

Composites	Average Particles Size (μm)	Density (g/cm^3)	RD	Porosity Fraction (%)
ACC212	254.234±10 %	1.88±0.05	0.693	30.63
ACC150	165.812±80 %	1.92±0.03	0.708	29.16
ACC100	120.658±12 %	1.98±0.04	0.731	26.94

The strength is one of the essential requirements of composites because bending or compression forces are often encountered during the service life of composites materials for any application. Therefore, the compressive strength of AC composites should be sufficient to avoid any form of structural damage. **Fig. 2 (c)** represent the strain-stress curve of ACC212, ACC150, and ACC100. From **Fig. 2 (c)** is clearly seen that stress-strain curve increases linearly up to the definite stress this is known as the plastic collapse of the composites. After the plastic collapse stress, nominal decreasing the stress in finding with a small bump and then increase in strain, stress oscillates with respect to the average stress line up to a certain known as densification strain [**31**]. This region is known as plateau region. After the plateau region, densification region starts, where the composite tends towards densified materials, and in this region stress increase linearly. **Fig. 2 (d)** shows the compressive strength of ACC212, ACC150, and ACC100. Initially, the compressive strength of ACC212 is 167.4MPa while in the case of ACC150 and ACC100 it increasing to 203.3 and 251.5MPa respectively. It was found that by decreasing the size of cenosphere, cenosphere cells gets smoothed and the number of cracks present on the surface gets reduce which results in the increasing the modulus thus the stress increasing. Furthermore, the increasing in the compressive strength with decreasing the size of cenosphere may also be due to lower inter-cenosphere spacing's which arrests dislocation motion, and also more uniform stress distribution. In case of coarser cenosphere, in addition to greater inter-cenosphere spacing's, the stress localization is more and the coarser cenosphere acts as larger crack size when starts deforming.

The EMI shielding effectiveness (SE) of a material is the ability to attenuate electromagnetic (EM) radiation that can be expressed in terms of the ratio of incoming (P_i) and outgoing (P_o) power [**32**].

$$SE_T(dB) = 10\log(P_o/P_i) \quad (1)$$

where, P_i and P_0 are the incidents and outgoing power, respectively. The EMI attenuation offered by a shield may depend on the three mechanisms: a reflection of the wave from the front face of the shield, absorption of the wave as it passes through the shield's thickness and multiple reflections of the waves at the various interface [**33**]. Therefore, SE_T of EMI shielding materials is determined by three losses i.e. reflection loss (SE_R), absorption loss (SE_A) and multiple reflection losses (SE_M), which can be expressed is as i.e.:

$$SE_T\,(dB) = SE_A + SE_R + SE_M \quad (2)$$

$$SE_R\,(dB) = -10\log\,(1 - R) \quad (3)$$

$$SE_A\,(dB) = -10\log\,(1 - A_{eff}) = -10\log\frac{T}{1-R} \quad (4)$$

$$SE_M\,(dB) = -20\log\,(1 - 10^{-SEA/10}) \quad (5)$$

where R and T are the reflectance and transmittance respectively. The contribution of SE_M is important for low absorbing materials and it can be ignored (SE_M~0) when SE_T of EMI shielding material is more than -10 dB and hence the total shielding effectiveness (SE_T) can be written as

$$SE_T(dB) = SE_R + SE_A \quad (6)$$

For reflection, the shield must have mobile charge carriers and tends to be electrically conducting. Although, not required very high conductivity. On the other hand absorption of the radiation by shield depends on electric and magnetic dipoles. Materials with high values of dielectric constant provide the electric dipoles while the materials having high values of magnetic permeability provides the magnetic dipoles.

The electromagnetic interference shielding of the aluminum alloy have been investigated by many authors. Dou et al.,[**13**] reported that aluminum 2024 alloy have EMI shielding -34 to -36 dB in the frequency range of 30 KHz to 1.5 GHz. Later on, Hu et al.,[**12**] investigate the effect of porosity on the EMI shielding performance of aluminum foam. The EMI shielding performance of these foam are in the range of -25 to -75 dB in the frequency range of 130-1800 MHz. In both the cases, in higher frequency range (1.5 and 1.8 GHz), the EMI shielding of aluminum alloy and foam is considerably low. Additionally, they also have not measured the contribution due to individual shielding component (reflection and absorption).

In the present investigation, cenosphere particles (high dielectric material) are incorporated in composites and their EMI shielding measurements are carried out in X-band frequency range (8.2−12.4 GHz). **Fig. 3 (a-c)** shows the results obtained by absorption, reflection and total EMI SE with frequency as a function of different size loading cenosphere in composites. When the electromagnetic wave falls on AC composites; the dominant loss of the incident electromagnetic wave is through reflection. The energy is consumed mainly due to magnetic and dielectric loss because of the presence of magnetic and dielectric material i.e. cenosphere. A small part of the incident electromagnetic wave is absorbed by composites material.

It is observed from **Fig. 3 (a)** that SE_T value of ACC212 is -32.7 dB at a thickness of 2.0 mm and SE_T is shared by SE due to the reflection (-20.5 dB) and absorption(-12.2 dB) at a frequency of 8.2 GHz. From these results, it clearly shows that ACC212 is dominated by reflection loss. From the experimental measurement, it is well evident that decreasing the size of cenosphere in ACC150 the total shielding effectiveness is increasing to -36.2 dB with decreasing the reflection loss (-17.4 dB) and increasing absorption loss (-18.8 dB) at frequency 8.2 GHz. Further decreasing the size of cenosphere particles in ACC100 the SE_T reaches to -44.3 dB, SE_T is shown absorption dominating nature (SE_A -31.1 dB) and reflection losses (SE_R -13.2 dB) at a frequency of 8.2 GHz. The cenosphere in the aluminum matrix results in the formation of more interfaces and a heterogeneous system creates the more interface space charge accumulation sites. Trapping of some polaron/bipolarons on cenosphere surface (due to the dielectric difference) and dielectric loss of SiO_2, Al_2O_3 (main constituents of cenosphere) could be considered as another reason for the improved results [**21**].

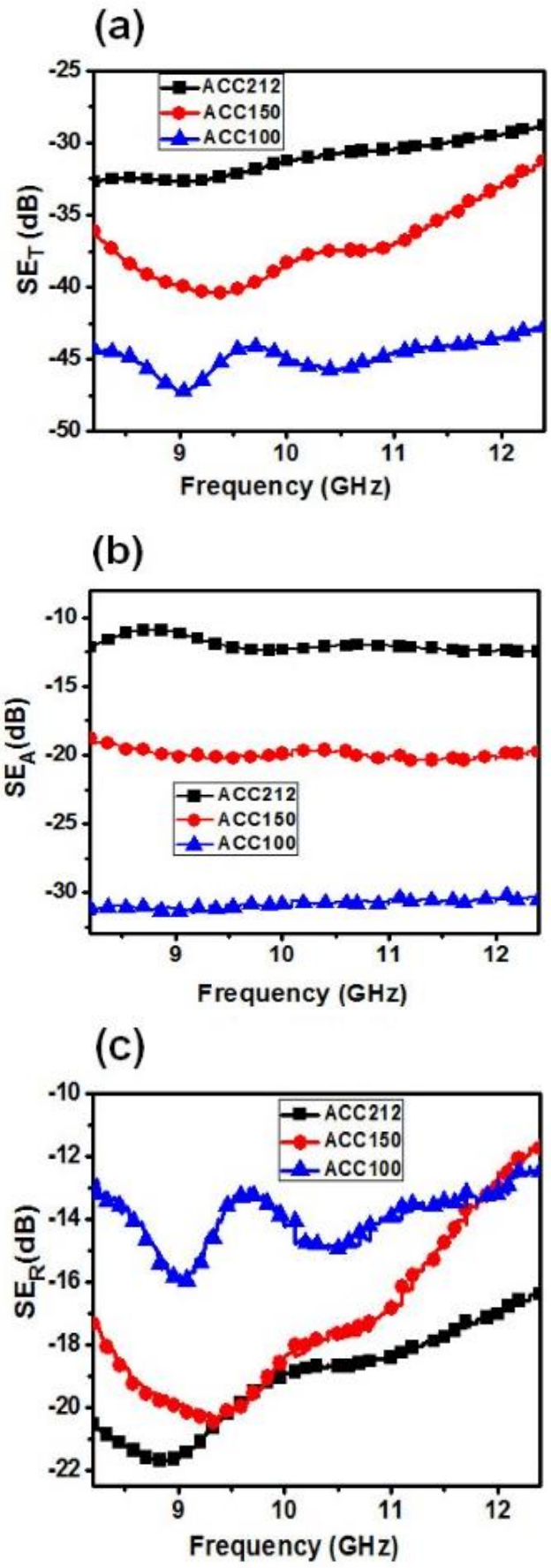

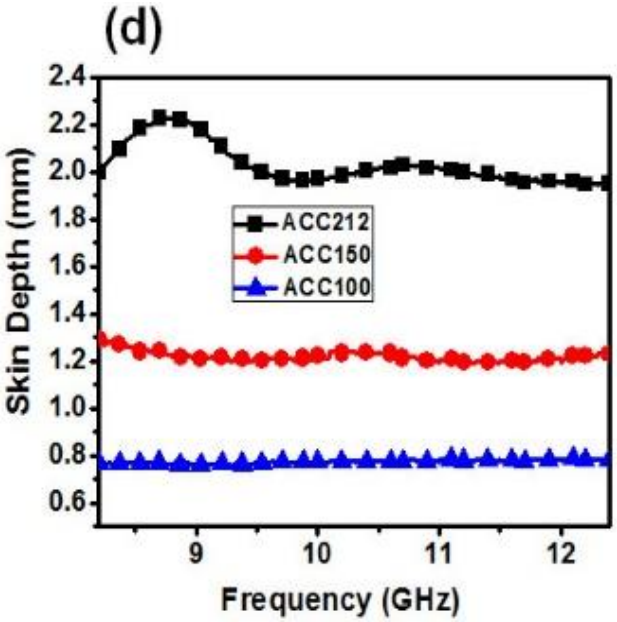

Fig. 3. EMI-SE of AC composites: (a) SE_T, (b) SE_R, (c) SE_A and (d) skin depth in the frequency range of 8.2 to 12.4 GHz (X-band) with decreasing size of cenosphere.

Accordingly, the results show that improved absorption and decreasing reflection with decreasing size of cenosphere particles **(Fig. 3 b and c)**, indicating that the dielectric nature and smaller size of cenosphere have a dominating role in electromagnetic attenuation. The smaller size of cenosphere fineness provides large surface area to the shielding material because of the presence of a large number of polaron at the surface of lower size cenosphere. Furthermore, the lower size of cenosphere is dispersed optimally in the aluminum matrix and the incident electromagnetic wave has to pass through scattering and thus loses energy which is absorbed by the composite (due to the heterogeneity of the system) and hence helping increase of SE_A. In addition, the synergetic effect in between aluminum and cenosphere might be conducive to the enhanced EMI SE.

The extreme change in reflection and absorption component (SE_R and SE_A) in ACC100 can be expressed as [**34**]:

$$SE_R\,(dB) = 108 + \log_{10}\left(\frac{\sigma}{f\mu}\right) \quad (7)$$

σ is electrical conductivity of shield material, hence reflection loss is directly proportional to conductivity.

$$SE_A(dB) = -8.68\left(\frac{t}{\delta}\right) = -8.68\alpha t \quad (8)$$

where 'α' is the attenuation coefficient which describes the extent to which the intensity of an electromagnetic wave is reduced when it passes through a specific material, t is the thickness and δ is the skin depth. The parameter skin depth (δ=1/α) is defined as the depth of penetration at which the incident EM radiation is reduced to 33% of its original strength, therefore, skin depth (δ) expressed as [**35**]:

$$\delta = \left(\frac{2}{f\mu\sigma}\right)^{1/2} = -8.68\left(\frac{t}{SE_A}\right) \quad (9)$$

where f is frequency, σ is electrical conductivity and μ is permeability and t is the thickness of composites. **Fig. 3 (d)** shows the variation in skin depth of AC composites with various size of cenosphere loading at frequency range 8.2 -12.4 GHz. From equation (ix), it is clearly observed that skin depth (δ) is inversely proportional to SE_A. Therefore, ACC212 having the maximum δ of 2.0 mm exhibits minimum absorption loss of -12.2 dB at a frequency of 8.2 GHz. Alternatively, ACC100

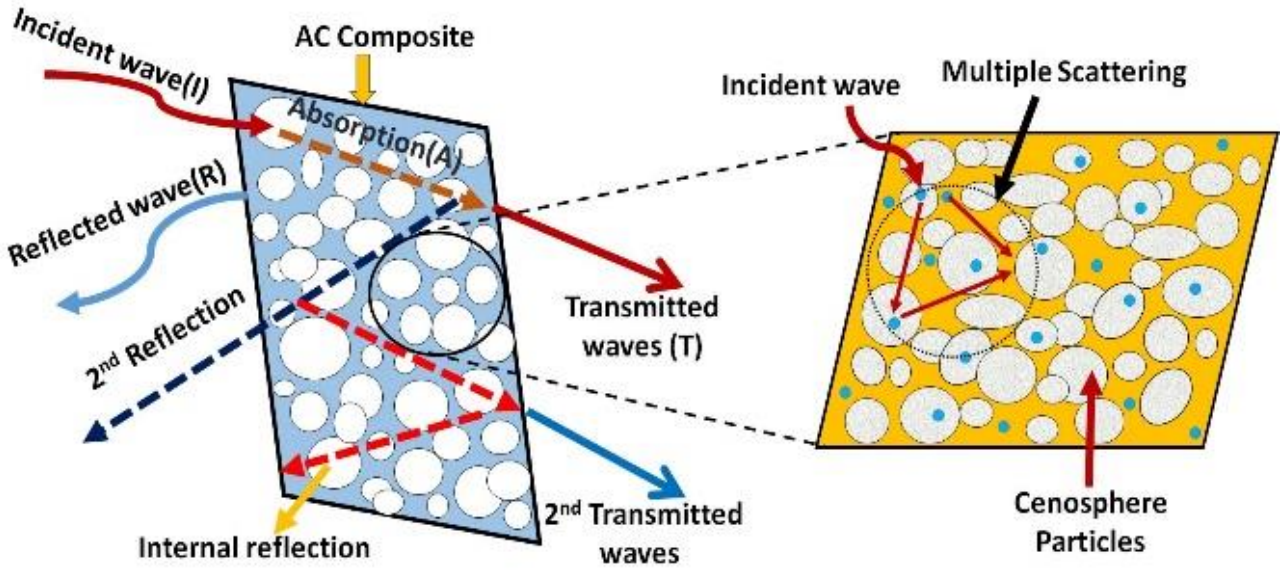

Fig. 4. Schematic representation of EMI shielding mechanism.

exhibiting maximum absorption loss of -31.1 dB with a minimum skin depth of 0.8 mm.

Now as we know, $\varepsilon_r = \varepsilon'$, $\tan\delta = \frac{\varepsilon'}{\varepsilon''}$ and $\sigma_T = (\sigma_{ac} + \sigma_{dc})\omega\varepsilon_0\varepsilon''$ we get $\tan\delta = \frac{\sigma_T}{\omega\varepsilon_0\varepsilon''}$ where σ_{ac} and σ_{dc} are frequency ($f = \omega/2\pi$) dependent (ac) and independent (dc) components of total microwave conductivity (σ_T) whereas ε' and ε'' represent dielectric constant and dielectric loss.

$$\lambda_0 = \frac{2\pi c}{\omega} = \frac{2\pi}{\omega\sqrt{(\varepsilon\mu)}} = \frac{2\pi}{\sqrt{(\varepsilon'\mu')(\varepsilon_0\mu_0)}} \quad (10)$$

The above equations reveal that for moderately conducting and non-magnetic materials ($\mu' \sim 1$ and $\mu'' \sim 0$) [**36**], i.e. both electrical conductivity as well as dielectric constant are important for suppression of reflection and parallel enhancement of absorption loss. Therefore, incorporation of high dielectric constant lower size spherical particles like cenosphere within conducting aluminum matrix is expected to enhance the overall attenuation. The interaction of electromagnetic waves with composite is shown in a schematic diagram **(Fig. 4)**.

The relative complex dielectric parameters ($\varepsilon^* = \varepsilon' - i\varepsilon''$) have been estimated from experimental scattering parameters (S11 & S21) obtained by standard Nicholson–Ross and Weir algorithm [**37, 38]**. The estimated dielectric constant (ε′) symbolizes the amount of polarization occurring in the material or the storage ability of the electrical energy, while the dielectric loss (ε″) signifies the dissipated electrical energy. The frequency dependence of ε′ and ε″ in the X band (8.2 to 12.4 GHz) for all composites is plotted in **Fig. 5 (a) and (b)**. The presence of doping induced localized charges on the aluminum matrix gives pronounced/strong polarization effects [**1**]. Additionally, dielectric performance of the material depends on electronic, ionic, orientation and space charge polarization. The contribution to the space charge polarization appears due to the heterogeneity of the material. The presence of dielectric materials (cenosphere) in high conducting aluminum results in the formation of more interfaces and a heterogeneous system due to some space charge accumulating at the interface that contributes toward the higher microwave absorption in the composites.

From **Fig. 5 (a)**, it can be observed that the ε′ of composites increases with decreasing the size of cenosphere. The values of ε′ at fixed frequency of 8.2 GHz are 60.1, 66.0 and 71.9 for ACC212, ACC150 and ACC100 respectively. In ACC100, ε′ is higher than that of ACC150 and ACC212. However, in **Fig. 5 (b)** the values of ε″ at a fixed frequency of 8.2 GHz are 42.7, 46.0 and 51.9 for ACC212, ACC150, and ACC100 respectively. Similarly, in ACC100, the value of ε″ is also higher as than that of ACC150 and ACC212. It is proposed that the decreasing size of cenosphere increases the interfacial polarization [**39, 40]**. Additionally, the increasing the value of ε′ and ε″ of ACC100 is mainly because of more uniform distribution and large surface area of lower size cenosphere (+100 μm) than bigger size (+212 μm). This gives effective much interaction between the lower size cenosphre particles and the aluminum matrix. Apart from this, the dielectric losses and high thermal stability of SiO_2, Al_2O_3 in cenosphere play a critical role for the investigated results.

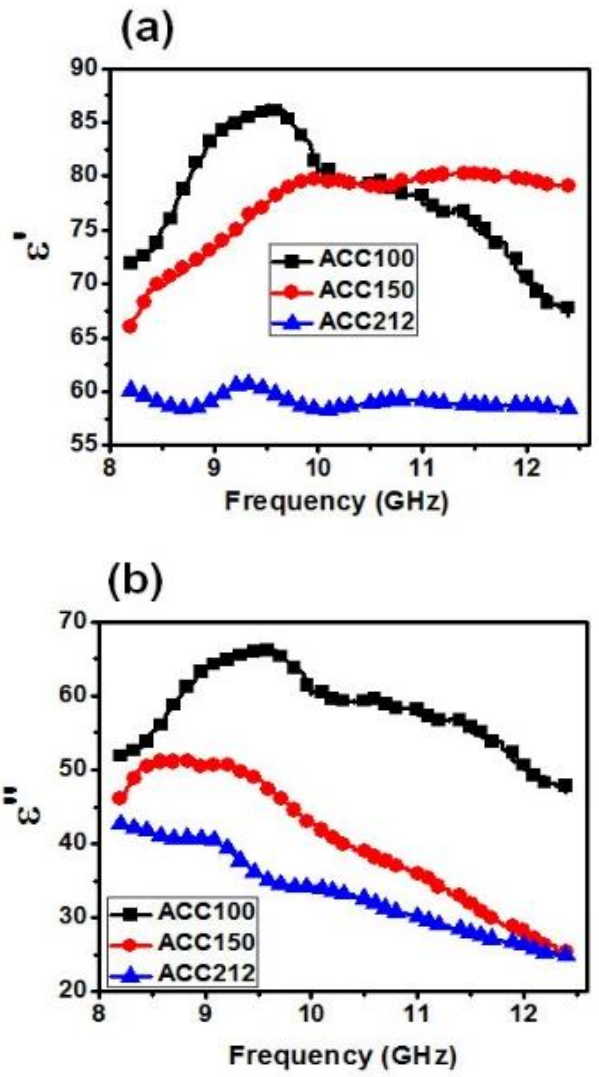

Fig. 5. Frequency dependence of (a) dielectric constant (ε′) and (b) dielectric loss (ε″) of AC composites.

Conclusion

In summary, a novel approach is used to fabricate AC composites by modified stir casting technique which shows promising EMI shielding properties in X band (8.2-12.4 GHz). The most effectiveness EMI shielding effectiveness was obtained for composites with +100μm cenosphere (ACC100), -44.3 dB and the EMI shielding due to absorption was found to be high -31.1 dB. The reflection component was reduced by fly ash based cenosphere but to reduce further, a considerable amount of research is still required. In future, we need to add magnetic and dielectric filler to achieve minimum reflection component. The high value of absorption component by industrials waste materials (cenosphere)

could be one of the best candidates for EMI shielding applications as compared to other conventional materials. Moreover, the compressive strength of ACC100 was found 251.3 MPa that indicates composites is particularly suitable for civil and military aerospace industry.

Acknowledgements

Authors are highly grateful to the Director, CSIR-AMPRI to publish the results. The authors are also thankful to Deepak Kashyap for SEM characterization. Authors also wish to thank Mr. Prasanth N. for XRD and compressive strength measurements. The authors would like to thanks, Madhya Pradesh Council of Science & Technology (MPCST) for financial supports and the author Rajeev Kumar thankful to DST, Govt. of India for Inspire Faculty Programme.

Author's contributions

Conceived the plan: R. Kumar, D. Mondal, S. Das; Performed the expeirments: A.Vishvakarma, S. Birla; Data analysis: R. Kumar, D. Mondal, A.Chaudhary, Saroj Kumari; Wrote the paper: Rajeev Kumar, D. Mondal. Authors have no competing financial interests.

Supporting information

Supporting informations are available from VBRI Press.

References

1. Chung, D. D. L; *J. Mater. Eng. Perform*., **2000**, *9*, 350. **DOI:** 10.1361/105994900770346042
2. Kumar, R.; Dhakate, S. R.; Saini, P.; Mathur, R. B; *RSC Adv*., **2013**, *3*, 4145. **DOI:** 10.1039/C3RA00121K
3. Zamanian, A.; Hardiman, C; *High Freq. Electron.*, **2005**, *4*, 16. **DOI:** 10.1.1.399.7869
4. Coleman, J. N.; Khan, U.; Blau, W. J.; Gun'ko, Y. K; *Carbon*, **2006**, *44*, 1624. **DOI:** 10.1016/j.carbon.2006.02.038
5. Chen, Z.; Xu, C.; Ma, C.; Ren, W.; Cheng, H. M; *Adv. Mater*., **2013**, *25*, 1296. **DOI:** 10.1002/adma.201204196
6. Tong, X. C; *Advanced materials and design for electromagnetic interference shielding*. CRC Press: **2016**. **DOI:**10.1201/9781420073591
7. Geetha, S.; Satheesh Kumar, K.; Rao, C. R.; Vijayan, M.; Trivedi, D; *J. Appl. Polym. Sci*., **2009**, *112*, 2073. **DOI:** 10.1002/app.29812
8. Cao, M.-S.; Wang, X.-X.; Cao, W.-Q.; Yuan, J; *J. Mater. Chem. C*, **2015**, *3*, 6589. **DOI:** 10.1039/C5TC01354B
9. Huang, H. D.; Liu, C. Y.; Zhou, D.; Jiang, X.; Zhong, G.J.; Yan, D. X.; Li, Z. M; *J. Mater. Chem. A*, **2015**, *3* 4983. **DOI:** 10.1039/C4TA05998K
10. Jamaati, R.; Toroghinejad, M. R; *Mater. Sci. Eng. A*, **2010**, *527*, 4146. **DOI:** 10.1016/j.msea.2010.03.070
11. Torralba, J.; Da Costa, C.; Velasco, F; *J. Mater. Process. Technol.*, **2003**, *133*, 203. **DOI:** 10.1016/S0924-0136(02)00234-0
12. Xu, Z.; Hao, H; *J. Alloys Compd*., **2014**, *617*, 207. **DOI:** 10.1016/j.jallcom.2014.07.188
13. Dou, Z.; Wu, G.; Huang, X.; Sun, D.; Jiang, L; *Compos. Part A: Appl. Sci. Manuf.*, **2007**, *38*, 186. **DOI**: 10.1016/j.compositesa.2006.01.015
14. Ohlan, A.; Singh, K.; Chandra, A.; Dhawan, S; *Appl. Phys. Lett*., **2008**, *93*, 053114. **DOI:** 10.1063/1.2969400
15. Xu, H.; Zhang, H.; Lv, T.; Wei, H.; Song, F; *Colloid Polym. Sci*., **2013**, *291*, 1713. **DOI:** 10.1007/s00396-013-2906-0
16. Singh, K.; Ohlan, A.; Saini, P.; Dhawan, S; *Polym. Adv. Technol*., **2008**, *19*, 229. **DOI:** 10.1002/pat.1003
17. Zhou, M.; Zhang, X.; Wei, J.; Zhao, S.; Wang, L.; Feng, B; *J. Phys. Chem. C*, **2010**, *115*, 1398. **DOI:** *10.1021/jp106652x*
18. Kong, L.; Yin, X.; Ye, F.; Li, Q.; Zhang, L.; Cheng, L; J. Phys. Chem. C, 2013, *117*, 2135. **DOI:** 10.1021/jp309984p
19. Kumar, R.; Singh, A. P.; Chand, M.; Pant, R. P.; Kotnala, R. K.; Dhawan, S. K.; Mathur, R. B.; Dhakate, S. R; *RSC Adv.*, **2014**, *4*, 23476. **DOI:** 10.1039/C4RA01731E
20. Yan, L.; Wang, J.; Han, X.; Ren, Y.; Liu, Q.; Li, F; *Nanotechnology*, **2010**, *21*, 095708. **DOI:** 10.1088/0957-4484/21/9/095708
21. Singh, A. P.; Kumar, A.; Chandra, A.; Dhawan, S; *AIP Adv*., **2011**, *1*, 022147. **DOI:** 10.1063/1.3608052
22. Bora, P. J.; Mallik, N.; Ramamurthy, P. C.; Madras, G; *Compos. Part B: Eng*., **2016**, *106*, 224. **DOI:** 10.1016/j.compositesb.2016.09.035
23. Yu, X.; Shen, Z; *J. Magn. Magn. Mater*., **2009**, *321*, 2890. **DOI:** 10.1016/j.jmmm.2009.04.040
24. Sambyal, P.; Singh, A. P.; Verma, M.; Gupta, A.; Singh, B. P.; Dhawan, S; *Adv. Mater. Lett.*, **2015**, *6*, 585. **DOI:** 10.5185/amlett.2015.5807
25. Iyer, R.; Scott, J; *Resour. Conserv. Recycl.*, **2001**, *31*, 217. **DOI**: 10.1016/S0921-3449(00)00084-7
26. Fenelonov, V. B.; Mel'gunov, M. S.; Parmon, V. N; *Powder Part. J.*, **2010**, *28*, 189. **DOI:** 10.14356/kona.2010017
27. Bora P.J.; Vinoy K.; Ramamurthy P.C.; Madras G; *Mater. Res. Express*, **2015** 2, 036403. **DOI:** 10.1088/2053-1591/2/3/036403
28. Wu G.; Huang X.; Dou Z.; Chen S.; Jiang L; *J. Mater Sci*., **2007**, *42*, 2633. **DOI:** 10.1007/s10853-006-1347-2
29. Ngu, L.N.; Wu, H.; Zhang, D.K; *Energy Fuels*, **2007**, *21*, 3437. **DOI:** 10.1021/ef700340k
30. Mondal, D.; Das, S.; Ramakrishnan, N.; Bhasker, K. U; *Compos. Part A: Appl. Sci. Manuf.*, **2009**, *40*, 279. **DOI:** 10.1016/j.compositesa.2008.12.006
31. Mondal, D.; Goel, M.; Das, S; *Mater. Sci. Eng. A*, **2009**, *507*, 102. **DOI:** 10.1016/j.msea.2009.01.019
32. Saini, P.; Choudhary, V.; Singh, B.; Mathur, R.; Dhawan, S; Mater. Chem. Phys., **2009**, *113*, 919. **DOI:** 10.1016/j.matchemphys.2008.08.065
33. Kitaura, R.; Imazu, N.; Kobayashi, K.; Shinohara, H; *Nano Lett.*, **2008**, *8*, 693. **DOI:** 10.1021/nl073070d
34. Kumar, R.; Dhakate, S. R.; Gupta, T.; Saini, P.; Singh, B. P.; Mathur, R. B; *J. Mater. Chem. A*, **2013**, *1*, 5727. **DOI:** 10.1039/C3TA10604G
35. Chung, D; *Carbon* **2001**, *39*, 279. **DOI:** 10.1016/S0008-6223(00)00184-6
36. Agarwal P.R.; Kumar R.; Kumari S.; Dhakate S.R; *RSC Adv*., **2016**, *6*, 100713. **DOI:** 10.1039/C6RA23127F
37. Nicolson, A.; Ross, G; *IEEE Trans. Instrum. Meas*., **1970**, *19*, 377. **DOI:** 10.1109/TIM.1970.4313932
38. Weir, W. B; *Proc. IEEE*, **1974**, *62*, 33. **DOI:** 10.1109/PROC.1974.9382
39. Yang, Y.; Gupta, M. C.; Dudley, K. L.; Lawrence, R. W; *Nano Lett.* **2005**, *5*, 2131. **DOI:** 10.1021/nl051375r
40. Saini, P.; Arora, M.; Gupta, G.; Gupta, B. K.; Singh, V. N.; Choudhary, V; *Nanoscale* **2013**, *5*, 4330. **DOI:** 10.1039/C3NR00634D

